

Electron bunch trapping and compression by an intense focused pulse laserQ. Kong,^{1,2,*} S. Miyazaki,^{1,†} S. Kawata,¹ K. Miyauchi,¹ K. Sakai,¹ Y. K. Ho,² K. Nakajima,³ N. Miyanaga,⁴ J. Limpouch,⁵ and A. A. Andreev⁶¹*Department of Electrical and Electronic Engineering, Utsunomiya University, Yohtoh 7-1-2, Utsunomiya 321-8585, Japan*²*Institute of Modern Physics, Fudan University, Shanghai 200433, China*³*High Energy Accelerator Research Organization, 1-1 Oho, Tsukuba, Ibaraki 305-0801, Japan*⁴*Institute of Laser Engineering, Osaka University, Yamada-oka 2-6, Suita, Osaka 565-0871, Japan*⁵*Institute of Physics/Czech Technical University, Academy of Sciences of the Czech Republic, CZ-182 121 Praha 8, Czech Republic*⁶*Research Institute for Laser Physics, Scientific Center, "S.I. Vavilov State Optical Institute," 199034, 12 Birzhevaya line, St. Petersburg, Russia*

(Received 25 December 2003; published 13 May 2004)

A focused short-pulse laser of TEM (1,0)+TEM (0,1) mode has two intensity peaks in the radial direction, so that the transverse ponderomotive force may trap electrons between the two peaks. At the same time the longitudinal ponderomotive force may accelerate electrons at the head of the laser pulse, when the laser is focused. When the electrons move to the laser tail, the laser may diverge and the electron deceleration becomes relatively weak. Our numerical analyses demonstrate that electrons are trapped well by the laser potential well, and that at the same time the acceleration by the longitudinal ponderomotive force induces the electron bunch compression. This trapping and compression mechanism is unique: the electron bunch can be compressed to the scale of the laser pulse length.

DOI: 10.1103/PhysRevE.69.056502

PACS number(s): 41.75.Jv, 42.50.Vk

I. INTRODUCTION

Intensive research works led to the remarkable development of laser chirped pulse amplification (CPA) technique [1–4], which has made TW compact short-pulse lasers available in laboratories. Current laser intensities reached to 10^{21} W/cm². It is expected that laser intensity of 10^{22} W/cm² or more is expected to be achieved in the near future. Such intense lasers can provide a field gradient of 10^6 – 10^7 MV/m, which is much higher than that of conventional accelerators, which is less than 100 MV/m. Thus laser acceleration of particles, especially electrons, has attracted significant research attentions [5–15]. A large number of theoretical and experimental advances have been performed in this field [8–17]. The laser acceleration schemes include the far-field acceleration scheme, i.e., free electron interaction with a propagating electromagnetic pulse wave, including laser, in vacuum.

In the laser acceleration in vacuum, there have been long-standing problems: one of the serious problems is the electron scattering in the perpendicular direction to a laser axis. Because the strong laser electric field component is in the transverse direction, it may drive electrons from the laser center. Consequently the electrons are expelled from the strong-field region quickly, lose a chance of full acceleration, and may also be led to an unacceptable radial spread [18]. This transverse scattering can be avoided or be weakened by creating a potential well in the radial direction [17–22]. Recently, Stupakov and Zolotarev [22] proposed an interesting

electron acceleration mechanism in vacuum with a linear combination of lasers of the TEM (0,0) mode and the TEM (1,0) and TEM (0,1) modes. In their scheme the electron bunch is confined by the radial potential well provided by the TEM (0,1) and TEM (1,0) modes and accelerated by the TEM (0,0) mode laser. One may imagine that a TEM (1,0)+TEM (0,1) mode of short-pulse laser may accelerate electrons by the longitudinal ponderomotive force in the longitudinal direction, in addition to the electron transverse confinement by the transverse ponderomotive force. We also studied the ponderomotive acceleration by the TEM (1,0)+TEM (0,1) mode laser [17].

In this paper, we present electron dynamics in the laser electron acceleration by the TEM (1,0)+TEM (0,1) mode laser: electrons are trapped by the radial ponderomotive potential well of the laser pulse for a long time, and accelerated well at the same time, and the electron beam bunch is compressed in longitudinal to the size of the laser pulse. In this electron trapping and compression mechanism electrons can interact for a long time with the laser field due to the laser confinement effect: for example, for $a_0 \equiv eE_0/m_e c \omega = 10$ (where a_0 is the dimensionless parameter specifying the magnitude of the laser field, $-e$ and m_e are the electron charge and mass, respectively, c the speed of the light in the vacuum, and ω the light angular frequency) the electron can get the maximum energy of 228 MeV from the TEM (1,0)+TEM (0,1) mode laser, while the maximum energy is 38.9 MeV in the case of the TEM(0,0) laser electron acceleration. In this paper, we present this trapping and acceleration scheme and the properties of the accelerated and compressed electron bunch in detail.

In the following, we present the laser field of TEM (1,0)+TEM (0,1) mode and our simulation model, and discuss on the mechanism of electron trapping and compression

*Corresponding author. Electronic address:

qkong@cc.utsunomiya-u.ac.jp

†Electronic address: kwt@cc.utsunomiya-u.ac.jp

scheme. Then we analyze the characteristics of the trapped and longitudinal compressed electron bunch.

II. LINEAR COMBINATION OF TWO HERMIT-TEM MODES

The transverse electric field of a TEM laser, propagating along the $+z$ direction, can be described by a linear combination of $E^{l,m}$ [23],

$$E^{i,m} = \text{Re} E_0^{l,m} H_l \left(\frac{\sqrt{2}x}{w(z)} \right) H_m \left(\frac{\sqrt{2}y}{w(z)} \right) \frac{w_0}{w(z)} \exp \left(-\frac{r^2}{w(z)^2} \right) \times \exp \left(i \left[kz - \omega t - (l+m+1)\varphi(z) \right] + \frac{kr^2}{2R(z)} \right), \quad (1)$$

where $E_0^{l,m}$ is the amplitude of the electric field, w_0 the beam width at the focus point, k the laser wave number, and H_l is the Hermite polynomial. $r = \sqrt{x^2 + y^2}$ is the transverse radius, and

$$w(z) = w_0 \left(1 + \frac{z^2}{Z_R^2} \right)^{1/2}, \quad (2)$$

$$R(z) = z \left(1 + \frac{Z_R^2}{z^2} \right), \quad (3)$$

$$\varphi(z) = \tan^{-1}(z/Z_R) \quad (4)$$

are the beamwidth, the curvature radius, and the Gouy phase factor of the laser beam, respectively. $Z_R = kw_0^2/2$ is the Rayleigh length. Thus, for $l=m=0$ it gives a laser of TEM (0, 0) mode, which is widely used in the literatures on the interaction between laser and matter.

The laser we employed is a short-pulse laser of a combination of the (1,0) mode ($l=1, m=0$) and the (0,1) mode ($l=0, m=1$). For the sake of simplification, we call it just the TEM (1, 0)+(0, 1) mode. The transverse electric field component for the TEM (1, 0)+(0, 1) mode is

$$E_r = 2\sqrt{2}E_0 r \frac{w_0}{w(z)^2} \exp \left(-\frac{r^2}{w(z)^2} \right) \times \exp \left\{ i \left[kz - \omega t - 2\varphi(z) + \frac{kr^2}{2R(z)} \right] \right\} f(\eta), \quad (5)$$

where $f(\eta)$ represents the Gaussian pulse envelop:

$$f(\eta) = \exp \left[-\left(\frac{\eta}{L_z} \right)^2 \right]. \quad (6)$$

Here L_z is the pulse duration and $\eta = z - ct$. The other electric and magnetic components can be obtained by using

$$E_z = \left(\frac{i}{k} \right) \left(\frac{\partial E_x}{\partial x} + \frac{\partial E_y}{\partial y} \right), \quad \mathbf{B} = -\left(\frac{i}{\omega} \right) \nabla \times \mathbf{E}. \quad (7)$$

The paraxial approximation [24,25] is used to derive full expressions of the electric and magnetic fields. The approximation was proved to work well for a large focus scale of $kw_0 > 50$ [26]. We can obtain the fields of a pulsed laser in

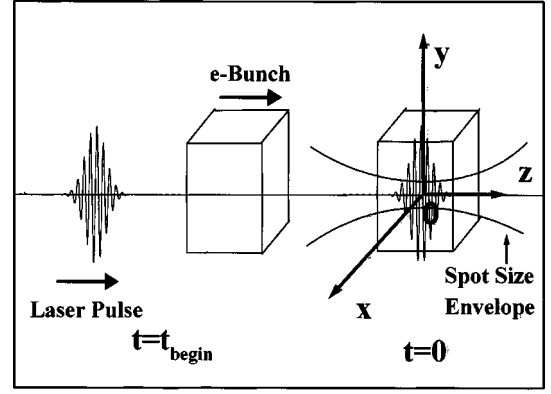


FIG. 1. Configuration of the electron trapping and acceleration in vacuum by TEM (1,0)+(0,1) mode laser. The laser and the injected electron bunch propagate along the z axis. The electrons do not experience the laser field initially at $T = T_{begin}$. The center of the laser pulse and the electron bunch coincide with each other at the laser focus at $T = 0$.

the TEM (1, 0)+(0, 1) mode from Eqs. (5)–(7).

On the other hand the Maxwell equation requires the symmetry of the electric components and the magnetic components. However, from Eq. (7), one can find terms $(\partial f / \partial z) E_x$ and $(\partial f / \partial z) E_y$ appearing in B_x and B_y , and these terms break the symmetry of \mathbf{E} and \mathbf{B} . For a long-pulse laser or a stationary laser, i.e., $L_z \rightarrow \infty$, these terms can be neglected, and Eqs. (5)–(7) provide a good approximation. However for a short-pulse laser, such as a pulse duration concerned in this paper, e.g., $L_z \leq 10\lambda$, the contribution of these terms cannot be ignored, and the terms may lead to an overestimation of the energy exchange between the electrons and the laser. To avoid the model error, we follow the idea of Davis [25] to find the symmetric field description for the laser field. Equations (5)–(7) are combined with the field description starting from the magnetic field as follows:

$$B_x = -E_y, \quad B_y = E_x, \quad B_z = -\left(\frac{i}{\omega} \right) \left(\frac{\partial B_x}{\partial x} + \frac{\partial B_y}{\partial y} \right), \quad (8)$$

$$\mathbf{E} = -\frac{i}{\omega} (\nabla \times \mathbf{B}).$$

Equations (5)–(7) and Eq. (8) are summed and divided by 2. This model ensures the field symmetry and serves a reasonable interaction between electrons and laser, as shown below.

The configuration of our electron bunch acceleration scheme is shown in Fig. 1. The laser pulse propagates along the z axis from the position of the minus in z and impinges on the electron beam. We set the beginning time of the simulation at $T_{begin} < 0$, when the electrons do not experience the laser field. At $t = 0$, the center of the laser pulse coincides with the electron beam center at the focus point.

The relativistic Newton-Lorentz equation of motion

$$\frac{d\mathbf{P}}{dt} = -e(\mathbf{E} + \boldsymbol{\beta} \times \mathbf{B}) \quad (9)$$

is solved to obtain the electron motion by the fourth-order Runge-Kutta method, where $\mathbf{P} = \gamma m \mathbf{V}$ and γ the Lorentz factor measuring the electron energy.

In the following, the laser wavelength λ is $1.053 \mu\text{m}$. Laser intensity I_0 is given in terms of the dimensionless parameter a_0 : $I_0\lambda^2 \sim (1.37 \times 10^{18})a_0^2$ for the TEM (0,0) mode and $I_0\lambda^2 \sim (5.48 \times 10^{18})a_0^2$ for the TEM (1,0)+(0,1) mode, when I_0 is expressed in W/cm^2 and λ in μm .

III. PONDEROMOTIVE ACCELERATION IN THE SHORT-PULSED LASER FIELD

A. Energy exchange between laser and free electron

In the research area of laser electron acceleration in vacuum, there has been a long-standing debate whether a free electron can obtain net energy from the laser field in vacuum. Every scheme on laser electron acceleration in vacuum needs confront this question. Since a laser beam in the lowest approximation can be considered as a plane wave, we first review the main results of the plane wave. For a plane wave propagating along the $+z$ direction with the vector potential $A_x(z-ct)\mathbf{e}_x$, one can obtain the field components:

$$E_x = -\frac{1}{c} \frac{\partial A_x}{\partial t},$$

$$B_y = \frac{\partial A_x}{\partial z} = E_x. \quad (10)$$

Assume that an electron moves in the z direction with the initial velocity $\beta_0 = \beta_z = v_0/c$ and the electron initial energy $\gamma_0 = (1 - v_0^2/c^2)^{-1/2}$. The electron oscillates in the laser field and shows a “quivering motion” in a transverse plane wave:

$$p_x = mcA, \quad p_y = 0, \quad p_z = mc\gamma_0 \left(\frac{1 + \beta_0}{2} A^2 + \beta_0 \right), \quad (11)$$

where $A = eA_x/m_e c^2$. During the oscillation, the electron energy varied between γ_0 and the maximum value of $\gamma \approx \gamma_0[(1 + \beta_0^2)A^2/2 + 1]$. If $A \gg 1$, the electron is accelerated to a relativistic energy. Because the light speed in vacuum is always larger than the electron speed, there exists a phase slippage between the laser and the electron. Due to the periodicity of the laser phase, the electron may be accelerated and decelerated alternately by the plane wave. In other words, any energy gain is temporary. This is usually concluded as the “Lawson-Woodward” theorem [27,28]. This result also stands for the case of a wave pulse of nonfocused laser. The electron gains energy at the head of the laser pulse and is decelerated at the tail of the pulse. After the wave overtakes and passes over the electron, the net energy gain is still zero.

In order to obtain a net energy, we need some ideas: for example, setting a boundary to separate accelerated electrons from laser, using the nonlinear ponderomotive force, and so on. In this paper we employ the ponderomotive force to accelerate electrons. In this acceleration mechanism one has to take into account a focusing effect of a focused pulse laser, like the laser shown in Eq. (1). As shown in Fig. 2(a), the amplitude of the laser intensity increases to the maximum when it approaches to the focus plane, and then decreases as

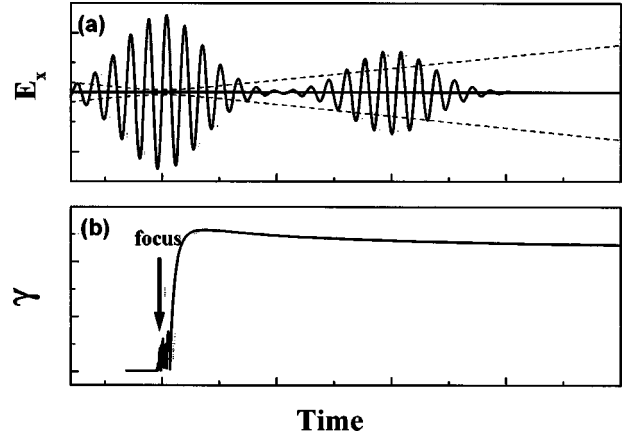


FIG. 2. The sketch map of the electron ponderomotive acceleration by an intense focused laser pulse. (a) The laser field intensity decreases quickly when the laser pulse leaves from the focus. The dashed line is the envelope of spot size. (b) An electron is accelerated near the focus and slightly loses its energy after the laser diffraction.

it leaves the focus plane. Therefore the electron may obtain a larger energy near the focus and lose a less energy at the deceleration phase, as shown in Fig. 2(b). This is the basic idea of the ponderomotive-force electron acceleration by an intense focused pulse laser.

With the theory of the ponderomotive potential model (PPM), it is easy to explain this laser acceleration mechanism in vacuum. In PPM, the time-averaged force experienced by an electron is given by $\mathbf{F}_{pond}(r, z, t) = -\nabla V_{pond}(r, z, t)$, where V_{pond} is the ponderomotive potential [29]:

$$V_{pond} = [\sqrt{1 + |\mathbf{A}(r, z, t)|^2/2} - 1]m_e c^2$$

$$\approx \begin{cases} [|\mathbf{A}(r, z, t)|^2/4]m_e c^2 & \text{if } |\mathbf{A}(r, z, t)| \ll 1 \\ [\sqrt{|\mathbf{A}(r, z, t)|^2/2}]m_e c^2 & \text{if } |\mathbf{A}(r, z, t)| \gg 1. \end{cases} \quad (12)$$

Here $|\mathbf{A}(r, z, t)|^2/2$ is the normalized time-averaged laser intensity profile. At the head of a pulse laser, the ponderomotive force $F_{pond} > 0$ and the electron absorbs the laser energy, while at the tail of the pulse $F_{pond} < 0$ and the electron loses its energy. For a plane-wave laser, the ponderomotive forces in these two stages are equal and the net energy exchange becomes zero. For a focused laser, F_{pond} in acceleration stage can be larger than that in the deceleration stage, and the electron can obtain the net energy after the interaction.

B. Electron scattering and trapping in focused short-pulse laser

Because the strong electric component of the laser is in the transverse direction, it leads to an electron scattering. For the widely used TEM (0,0) mode laser, the transverse electric component is

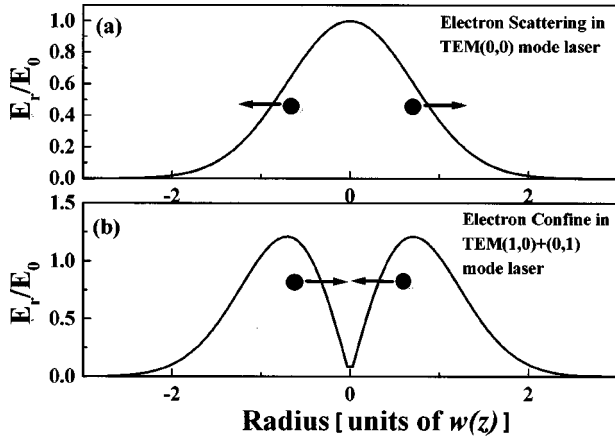


FIG. 3. The normalized intensity of transverse electric field E_r vs the radial radius r . (a) The electron transverse scattering in a TEM (0,0) mode laser. (b) Electron trapping in a TEM (1,0) + (0,1) mode laser.

$$E_r = E_0 \frac{w_0}{w(z)} \exp\left(-\frac{r^2}{w(z)^2}\right) \times \exp\left\{i\left[kz - \omega t - \varphi(z) + \frac{kr^2}{2R(z)}\right]\right\} \exp\left(-\frac{\eta^2}{L_z^2}\right). \quad (13)$$

This field has the maximum intensity at the center $r=0$ and decreases with r , as shown in Fig. 3(a). The corresponding normalized time-averaged laser intensity profile of this field is

$$A_0(r, z, t)^2 = a_0^2 \frac{w_0}{w(z)^2} \exp\left(-\frac{2r^2}{w(z)^2}\right) \exp\left(-\frac{2\eta^2}{L_z^2}\right). \quad (14)$$

One can obtain the transverse and longitudinal ponderomotive forces:

$$F_r = \frac{\sqrt{2}r}{w(z)^2} A_0(r, z, t), \quad (15)$$

$$F_z = \left[\left(1 - \frac{2r^2}{w(z)^2}\right) \frac{z/Z_R}{\sqrt{2}kw(z)^2} + \frac{\sqrt{2}\eta}{L_z^2} \right] A_0(r, z, t). \quad (16)$$

The transverse ponderomotive force F_r is always positive, which means that off-axis electrons are accelerated and scattered in transverse by the transverse force and are expelled from the strong field region. It is difficult for the scattered electrons to enter again into the near-axis region. In Eq. (16) we found that the longitudinal ponderomotive force F_z has two components: the first term $[1 - 2r^2/w(z)^2](z/Z_R)/\sqrt{2}kw(z)^2$ comes from the radial intensity gradient, i.e., the diffraction effect of a focused laser. It is clear that this term becomes negative, when $r > w(z)/\sqrt{2}$, and as a result the scattering electrons experience a distinct deceleration before they leave the laser beam. The second term $\sqrt{2}\eta/L_z^2$ comes from the intensity gradient of the laser pulse, where $\eta = z - ct$, which is the relative distance between the electron and the pulse center

of the laser. The second term denotes an acceleration force for $\eta > 0$ at the head of the laser pulse and a deceleration force for $\eta < 0$ at the tail of the laser pulse. Because $A_0(x, y, z, t)$ also has the diffraction effect, the second term can also lead to a net acceleration.

On the other hand, the axis-symmetric laser of TEM (1,0) + (0,1) mode defined by Eq. (5) has the minimum on the axis $r=0$ and has a peak at $r = w(z)/\sqrt{2}$. The corresponding normalized time-averaged laser intensity profile is

$$A_1^2(r, z, t) = 8a_0^2 \frac{w_0^2 r^2}{w(z)^4} \exp\left(-\frac{2r^2}{w(z)^2}\right) \exp\left(-\frac{2\eta^2}{L_z^2}\right). \quad (17)$$

The transverse and longitudinal ponderomotive forces are

$$F_r = \left(\frac{2r^2}{w(z)^2} - 1\right) a_0 \frac{2w_0}{w(z)^2} \exp\left(-\frac{r^2}{w(z)^2}\right) \exp\left(-\frac{\eta^2}{L_z^2}\right), \quad (18)$$

$$F_z = \left[\left(2 - \frac{2r^2}{w(z)^2}\right) \frac{z/Z_R}{kw(z)^2} + \frac{2\eta}{L_z^2} \right] a_0 \frac{2w_0 r}{w(z)^2} \times \exp\left(-\frac{r^2}{w(z)^2}\right) \exp\left(-\frac{\eta^2}{L_z^2}\right). \quad (19)$$

The transverse ponderomotive force of the TEM (1,0) + (0,1) mode laser is not always larger than zero. For electrons moving in the range of $r \in (0, \sqrt{2}w(z)/2)$, $F_r < 0$. The electrons can be driven to the center by the transverse ponderomotive force and may oscillate in this trap, as shown in Fig. 3(b). This trapping effect may provide an electron dynamics, in which the electrons can be kept inside the laser strong-field region for a longer time. Through this interesting electron dynamics, the electron transverse scattering can be avoided effectively, and therefore the electron bunch is confined and accelerated. In the longitudinal ponderomotive force the two terms $[2 - 2r^2/w(z)^2](z/Z_R)/kw(z)^2$ and $2\eta/L_z^2$ in Eq. (19) represent two sources of the electron net energy gain by the longitudinal ponderomotive force acceleration. Compared with the electron scattering feature of the TEM (0,0) mode laser, for electrons located in $r < w(z)$ the first term is positive, which means that the trapped electrons are accelerated successively by the longitudinal ponderomotive force, when they stay at the head of the laser pulse. This feature makes the longitudinal ponderomotive force acceleration notable. Because of the trapping effect, it is expected that the trapped electrons may interact with the TEM (1,0) + (0,1) laser for a longer time and that the electrons may obtain a higher net energy than that in the TEM (0,0) mode laser.

In spite of the trapping effect, electrons may experience the decrease in the field intensity as follows:

(1) electrons can move out from the region $r < w(z)$, because the field intensity decreases by $\exp[-r^2/w(z)^2]$.

(2) When electrons pass over the laser pulse, the field intensity decreases by the term $\exp(-\eta^2/L_z^2)$.

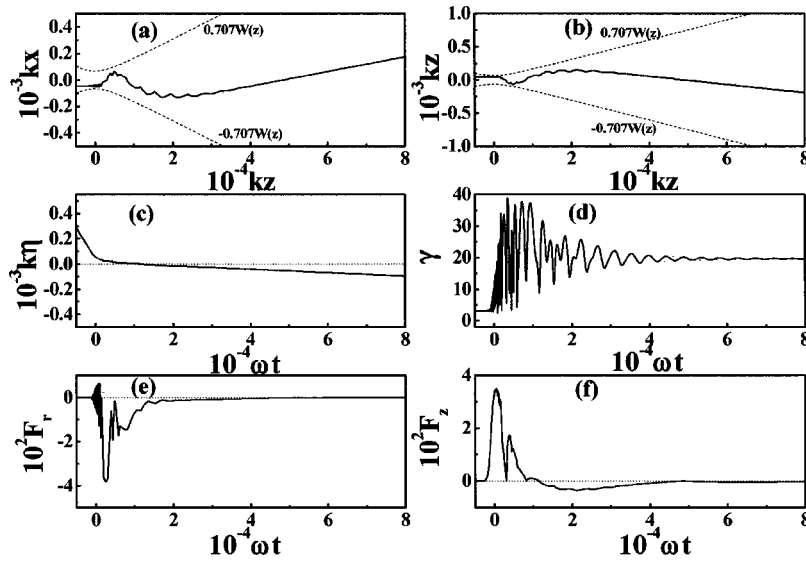


FIG. 4. A typical case of electron trapping and acceleration by a laser of TEM $(1,0)+(0,1)$ mode. The laser parameters are $a_0=3$, $w_0=15\lambda$, and $L_z=10\lambda$. The electron is injected at $kx_i=-44.6$, $ky_i=50.0$, and $kz_i=-29784$ with the initial velocity of $\beta_{xi}=\beta_{yi}=0.0$ and $\beta_{zi}=0.95$. (a) The electron trajectory in the x - z plane and (b) in the y - z plane. Here, the dashed lines represent the envelope of the radial potential well, $r=\pm w(z)/\sqrt{2}$. (c) The history of η , that is, the electron relative distance to the laser pulse center. (d) The energy history. (e) and (f) are the history of the transverse and longitudinal ponderomotive forces, respectively. The unit of the force in (e) and (f) is $m_e c^2/k$.

(3) The diffraction effect of a focused laser also contributes the electron scattering: the laser field intensity decreases by the term $1/w(z)^2$ for the TEM $(1,0)+(0,1)$ laser. In the electron scattering process in the TEM $(0,0)$ mode laser, most cases belong to the case (1), because in many cases electrons are scattered and the interaction time might not be sufficiently long. However, in the TEM $(1,0)+(0,1)$ mode laser the two terms of $[2-2r^2/w(z)^2](z/Z_R)/kw(z)^2$ and $2\eta/L_z^2$ are positive for the trapped electrons staying at the head of the laser pulse. Therefore if the electrons are accelerated to a speed close to the light speed c by a sufficiently intense laser or if the electron initial velocity is relativistic, the effective trapping and acceleration can be expected. If this situation is realized, a relative slippage between the laser pulse and the electrons may be slow. The electron can stay at the head of the laser pulse or near the center of the laser pulse, so that the electrons can be accelerated in longitudinal and trapped in transverse for a longer time. It can be also expected that a longitudinal compression phenomenon appears during the laser pulse illumination on the electron bunch. For these trapped and accelerated electrons, the main factor, led to the decrease in the laser intensity which the electrons see, is the factor $1/w(z)^2$ of case [3] shown above and is the slowest factor in time. Therefore during most of the interaction time of the trapped and accelerated electrons by the TEM $(1,0)+(0,1)$ laser, the longitudinal ponderomotive force is larger than zero. When the electrons move to the tail of the laser pulse and are decelerated, the laser may already diverge greatly and the laser intensity decreases much so that the deceleration can be minor.

Following the above discussions, the electron bunch we employed in our following analyses is in relativistic initially; the electron initial velocities are set to $\beta_{xi}=\beta_{yi}=0$, $\beta_{zi}=0.95$, corresponding to the initial energy of $\gamma_i=3.20$.

C. Electron dynamic trajectory in TEM $(1,0)+(0,1)$ mode laser

Complexity of the equation of motion and the field equations leaves little room for further analytic manipulations in drawing an intuitive picture. We therefore resort to numerical analyses below. First we analyze the characteristics of the electron dynamic trajectory in the laser of TEM $(1,0)+(0,1)$ mode.

In Fig. 4 we present a typical case for an electron trapping and acceleration in the laser of TEM $(1,0)+(0,1)$ mode with the parameters $a_0=3$, $w_0=15\lambda$, and $L_z=10\lambda$. The electron is injected from the $-z$ direction with the initial velocity of $\beta_{zi}=0.95$ and $\beta_{xi}=\beta_{yi}=0$. The initial position of the electron is $kx_i=-44.6$, $ky_i=50.0$, and $kz_i=-29784$. In Figs. 4(a) and 4(b), the electron trajectory in the x - z and y - z planes is presented. One can see that the electron is kept well in the potential well, i.e., $r \leq w(z)/\sqrt{2}$. Figure 4(c) shows the history of $\eta=z-ct$, that is, the relative longitudinal distance between the electron and the laser pulse center. At the beginning stage, η decreases quickly when the laser pulse approaches the electron. The electron stays at the head of the laser pulse till $\omega t \sim 11500$. Then the electron passes the laser pulse center and falls into the deceleration phase. Because of the relatively slow slippage between the electron and the laser pulse, this interaction stage lasts for a long time. The electron keeps inside the laser pulse until $\omega t \sim 50000$. The trapped electron is kept in the strong-field region and consequently accelerated well by the laser, as shown in Fig. 4(d), the maximum electron oscillation energy is $\gamma \approx 37.1$. After the deceleration stage, the final electron energy is $\gamma_f \approx 19.6$, corresponding to about 10.0 MeV. We found from the simulation that the electron energy becomes nearly constant after $\omega t > 60000$, the corresponding effective acceleration range is about 0.955 cm, and the accelera-

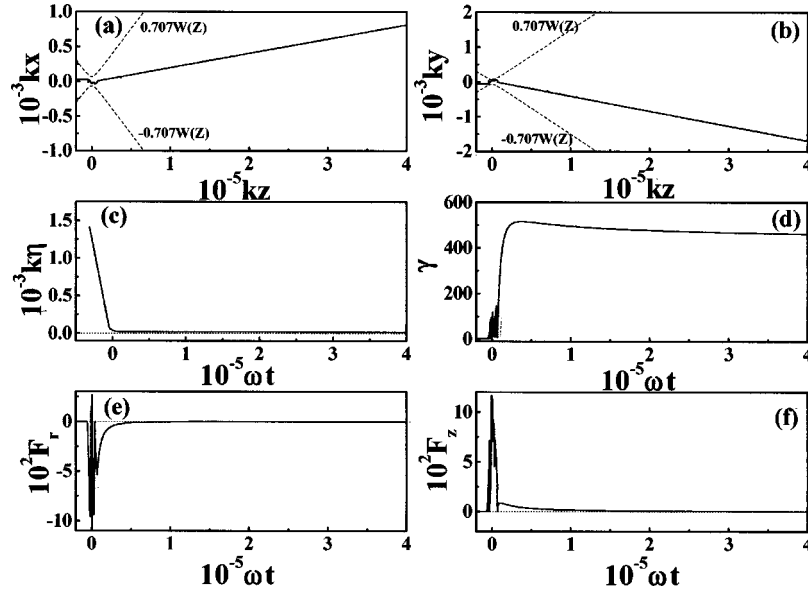


FIG. 5. A typical case of the electron trapping and acceleration in TEM (1,0)+(0,1) mode laser at the laser intensity of $a_0=10$. All parameters and figures are the same as in Fig. 4, expect the laser intensity and the electron initial position: $kx_0=-44.6$, $ky_0=50.0$, and $kz_0=-29\ 784$.

tion gradient reaches 1.47 GeV/m. The histories of the transverse and longitudinal ponderomotive forces shown in Figs. 4(e) and 4(f) prove our analyses discussed above. First, the transverse ponderomotive force is kept almost negative, because the electron is well trapped inside the range of $r \in [0, \sqrt{2}w(z)/2]$. Second, the longitudinal ponderomotive force is positive when the electron is kept at the head of the laser pulse, and after the electron passes the pulse center, it becomes negative which leads to a deceleration process. However, due to the diffraction effect of the focused laser, the deceleration is minor and the electron keeps the energy. Our calculation for an electron in the TEM (0, 0) mode laser with the same parameters shows that the electron final energy is about $\gamma_f \sim 9.37$ with the interaction time of $\omega t \sim 38\ 400$, which is much smaller than that in the TEM (1,0)+(0,1) mode laser.

The effects of the trapping and acceleration become more distinct, when the laser intensity increases. Figure 5 presents another result for the parameters $a_0=10$, $w_0=15\lambda$, and $L_z=10\lambda$ in the TEM (1,0)+(0,1) laser. The initial position of the electron is $kx_0=-44.6$, $ky_0=50.0$, and $kz_0=-29\ 784$. First, besides the electron transverse trapping phenomenon in Figs. 5(a) and 5(b), one can see in Fig. 5(c) that the electron is almost “captured” in longitudinal by the laser pulse. We found that the relative motion between the laser pulse and the electron becomes slower for $a_0=10$. In actual by the simulations we found that $\eta \geq 0$ is kept well until $\omega t = 1.60 \times 10^6$: at this time the electron longitudinal position is $\sim 180 Z_R$. The electron acceleration effect becomes more remarkable compared with the results in Fig. 4. The electron maximum oscillation energy is about $\gamma \sim 515$ and the final energy is about $\gamma_f \sim 447$, corresponding to 228 MeV. The simulation results for the TEM (0,0) laser electron acceleration with the same parameter values show that the final energy is about $\gamma_f \sim 76.2$, corresponding to 38.9 MeV. In Fig.

5(d) we can see that the decrease in the electron energy in the deceleration stage is small. The transverse ponderomotive force is almost negative and the longitudinal ponderomotive force is also almost positive. The longitudinal ponderomotive force accelerates the electron successively in longitudinal. The energy exchange becomes very small after $\omega t > 400\ 000$, corresponding to the acceleration distance of ~ 6.37 cm, and the acceleration gradient is about 3.58 GeV/m.

Through the analyses and simulations on the electron ponderomotive acceleration in the TEM (1,0)+(0,1) mode laser, we found that there are another electron dynamics besides the electron scattering in the Gauss mode laser. In this dynamic trajectory, the electron is trapped by the transverse potential well and kept at the head of the laser pulse for a long time. The trapped electron can be well accelerated by the longitudinal ponderomotive force and keeps the most of the oscillation energy. This trapped and acceleration effect becomes more remarkable, as the laser intensity increases. This scheme may have a potential to bring a compact high-energy electron-bunch generator.

IV. ELECTRON BUNCH TRANSVERSE CONFINEMENT AND LONGITUDINAL COMPRESSION

A. Electron bunch acceleration and its properties

Now we turn to study the characteristics of an accelerated electron bunch generated by this trapping and acceleration scheme. First we present an example to give a picture of the electron bunch acceleration process and the output electron bunch properties. The parameters of the laser employed here are $a_0=10$, $w_0=15\lambda$, and $L_z=10\lambda$. The corresponding laser intensity is $\sim 5.48 \times 10^{20}$ W/cm² for the laser wavelength $\lambda=1.053$ μm . The total number of the electrons used is 2.40×10^4 . Because the laser field is axially symmetric, we only present electron maps in the x - y plane (in Fig. 6) and

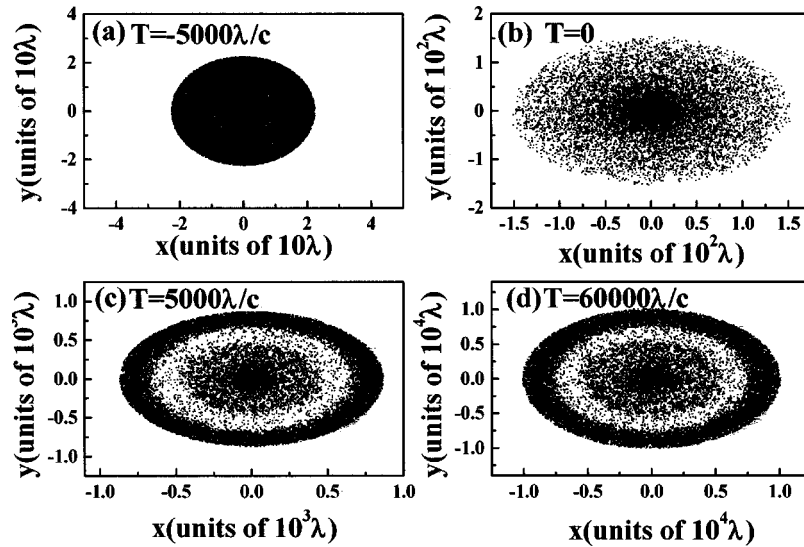


FIG. 6. Electron-bunch transverse confinement. The parameters are $a_0=10$, $w_0=15\lambda$, and $L_z=10\lambda$. Electrons are injected with the initial velocity of $\beta_x=\beta_y=0$, $\beta_z=0.95$. The electron maps on the transverse plane: (a) at the initial time of $T=-5000\lambda/c$, the electrons are located uniformly in the range of $r=\sqrt{x_i^2+y_i^2}\leq 1.5w_0$; (b) at $T=0$, the laser pulse bumps into the electron beam center; a high density electron group appears at the center; (c) at $T=5000\lambda/c$, many of electrons are trapped by the transverse potential well, while others be scattered; (d) at $T=60\,000\lambda/c$, electrons are divided into two groups: a trapped electron bunch located in the center and an annular scattered electron bunch located at $r>7500\lambda$.

the $x-z$ plane (in Fig. 7). The initial electrons are located uniformly inside the region of $r_i=\sqrt{x_i^2+y_i^2}\leq 1.50w_0$ and $T_{begin}\beta_{zi}-4L_z\leq z_i\leq T_{begin}\beta_{zi}+4L_z$ [see Figs. 6(a) and 7(a)]. The electron initial velocity is $\beta_{zi}=0.950c$ and the initial electron density is $1.74\times 10^{11}\text{ cm}^{-3}$. Both the electron bunch and the laser pulse are injected from the negative position in z . In our simulations the initial time means $T=T_{begin}=-5.00\times 10^3\lambda/c$.

There are two notable features in the electron bunch properties: one is the electron bunch transverse confinement by the transverse ponderomotive force; and another is the elec-

tron bunch longitudinal compression by the laser pulse. In Fig. 6 one can see that electrons injected into the region of $r_i\geq(\sqrt{2}/2)w_0$ are scattered, while other electrons injected into the potential well are driven to the center during the laser pulse overtaking the electrons. In this case, 3370 electrons are trapped inside the potential well $r_f\leq 900\lambda$ and most of these trapped electrons are located in the range of $r_f\leq 350\lambda$ at the final stage of $T=60\,000\lambda/c$. The most of the scattered electrons locate inside the region of $r_f\geq 7500\lambda$. It is clear that the TEM (1,0)+(0,1) mode laser achieves the electron-bunch confinement in radial.

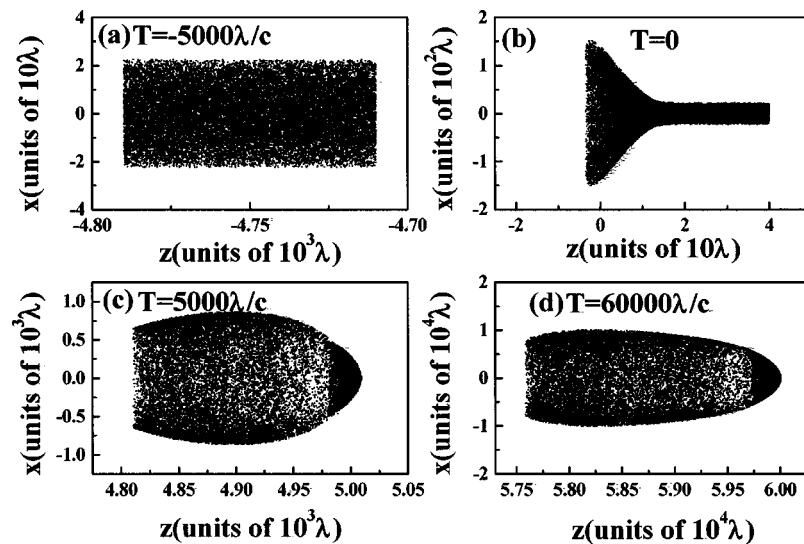


FIG. 7. Electron-bunch longitudinal compression. All the parameters are the same as in Fig. 6. The electron maps in the $x-z$ plane: (a) at the initial time of $T=-5000\lambda/c$; (b) at $T=0$ the center of the electron bunch and the laser pulse center coincide with each other; (c) at $T=5000\lambda/c$ some trapped electrons are overtaken by the laser pulse and move along with it; (d) at $T=60\,000\lambda/c$ a high-density electron bunch are generated by the longitudinal compression effect at the head of the electron pulse.

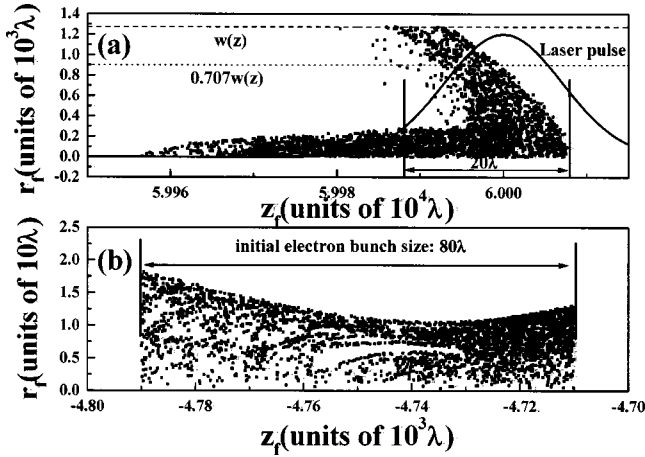


FIG. 8. The transverse confined and longitudinal compressed electron bunch. (a) Electron maps in the plane of z_f-r_f . The solid line is the sketch curve of the laser pulse, the dashed line is the longitudinal of the laser spot size, and the dotted line is the boundary of the radial potential well. The most part of the trapped electrons is located in the region $r < 300\lambda$ and $\Delta z \leq 20\lambda$. (b) The initial position of the accelerated and accumulated electrons belonging to the electron bunch in (a) in the z_f-r_f plane.

As we discussed in the preceding section, electrons irradiated by an intense laser as $a_0=10$, some electrons can be kept at the head of the laser pulse for a long time. Therefore while the laser pulse overtakes the electron bunch, more and more electrons are captured by the laser pulse: in other words, the laser pulse can assemble the electrons and form a high density electron bunch at the head of the laser pulse. This longitudinal compressed phenomenon is well revealed in Figs. 7 and 8. Figure 7(d); shows the electron bunch at the final stage of $T=60\,000\lambda/c$; 2579 electrons are located inside of the laser pulse length, i.e., 20λ , corresponding to 70 fs as shown in Fig. 8(a). Figure 8(b) shows the initial electron position map for the compressed and trapped electrons shown in Fig. 8(a), and one can find that these trapped and longitudinal compressed electrons are initially located from the head to the tail of the bunch. Based on this remarkable result for the laser electron bunch compression in longitudinal, we can expect that a larger number of electrons may be accumulated: in our simulations an electron bunch length of 80λ in z was limited by computer CPU and memory limitations. In an actual experiment one may use a longer electron bunch, so that more electrons can interact with and are accumulated by the short pulse laser. In addition, as we discussed above, the decrease in the laser field intensity in this acceleration scheme mainly comes from the term $1/w(z)^2$. This longitudinal bunch compression phenomenon may generate a high energy, short-pulse electron bunch in the scale of the laser pulse duration.

For the electron bunch located in the region of $r_f = \sqrt{x_f^2 + y_f^2} < w(z)/\sqrt{2} \approx 900\lambda$ and the longitudinal length 20λ , the transverse and longitudinal rms emittances are calculated by [22–30]

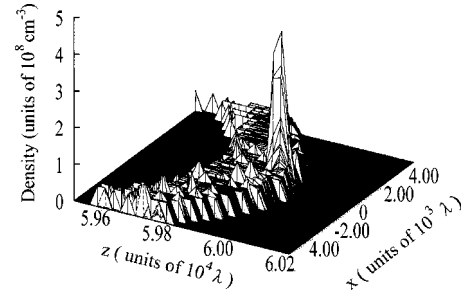


FIG. 9. The electron number-density distribution in the x_f-z_f plane. All the parameters are the same as those in Fig. 6.

$$\varepsilon_x = \left[\overline{(x - \bar{x})^2 (x' - \bar{x}')^2} - \overline{(x - \bar{x})(x' - \bar{x}')^2} \right]^{1/2},$$

$$\varepsilon_y = \left[\overline{(y - \bar{y})^2 (y' - \bar{y}')^2} - \overline{(y - \bar{y})(y' - \bar{y}')^2} \right]^{1/2}, \quad (20)$$

$$\varepsilon_z = \tilde{z} \frac{\Delta P_z}{P_z},$$

where $x' = dx/dz$ and $y' = dy/dz$ are the slopes of the electron trajectory, $z = s(t) - s_0(t)$ is the difference in the direction of the beam propagation, and $\Delta P_z = P_z - P_0$ is the difference of the momentum in the longitudinal direction. The $s(t)$ is the distance of particle transfer along the direction of beam propagation. P_0 is the average value of the longitudinal momentum. The rms emittances of the trapped electron bunch in Fig. 8 are $\varepsilon_x = \varepsilon_y = 0.129$ mm mrad and $\varepsilon_z = 4.27$ mm mrad, respectively.

In the following, we investigate the influence of the space charge (SC) effect. The SC effect is not included in our simulation model, because it is minor in our cases: the transverse electric field due to SC is $E_{\perp} \sim eN_e\gamma/2\pi L_z L_{\perp}$, where N_e is the electron number, L_z and L_{\perp} are the bunch sizes in longitudinal and transverse, respectively. Therefore the net SC force is $F_{\perp} \sim e^2 N_e / \gamma L_z L_{\perp}$. To avoid the emittances dilution by the SC effect, the relation $\Delta p_{\perp}^{(SC)} \sim F_{\perp} t \sim e^2 N_e m_e / 2\pi L_z p_{\perp} < p_{\perp}$ should be fulfilled. Then the maximum number limitation of electrons can be estimated by $N_e < (2\pi L_z / r_e)(p_{\perp} / mc)^2$, where p_{\perp} is the transverse momentum and r_e the classical electron radius. For the parameters we employed, $N_e \leq 1.59 \times 10^{10}$ and $n_e \leq 2.68 \times 10^{14} \text{ cm}^{-3}$ should be satisfied. Here n_e shows the electron number density. As shown in Fig. 9, the maximum electron density for the trapped electron bunch located at the head of the electron bunch and around the axis is about $5.0 \times 10^8 \text{ cm}^{-3}$ and the electron number in this example is about several thousands, that is, far less than the limit. Therefore the SC effect is minor in our simulations.

B. Energy distribution and spectra

We present the electron final energy γ_f versus the final longitudinal position r_f in Fig. 10(a) and versus the final transverse radius z_f in Fig. 10(b). One can see that there are two high-energy peaks in Fig. 10(a): one is located near the center and is the trapped electron group. Another is located around $r_f \sim 2000$ and consists of the electrons fleeing from

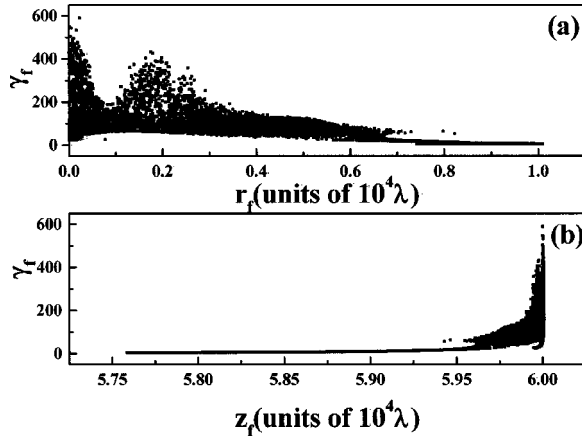


FIG. 10. The electron maps in the plane of the electron final energy γ_f vs (a) the electron final transverse distance $r_f = \sqrt{x_f^2 + y_f^2}$ and (b) the final electron longitudinal position z_f .

the potential well during the acceleration process. The final energies of the scattering electrons, located in the range of $r_f > 7500$, are very low, less than $\gamma_f \sim 50$. In Fig. 10(b) it is found that almost all high-energy electrons are located at the head of the electron bunch. Our calculation results show that the average final energy for the total electron bunch is about $\gamma \sim 36.8$, corresponding to about 18.8 MeV. The average final energy of the trapped electrons is $\gamma_f \sim 113$, corresponding to 57.7 MeV. The maximum electron energy is $\gamma_{f \max} \sim 590$, i.e., 301 MeV.

We present the energy spectra of the accelerated electrons in Fig. 11. One can see that these electrons are divided into two parts. The lower energy peak is located near $\gamma_f \sim 5$, which represents the scattered electrons. The higher-energy electrons have a relatively wide energy distribution and the

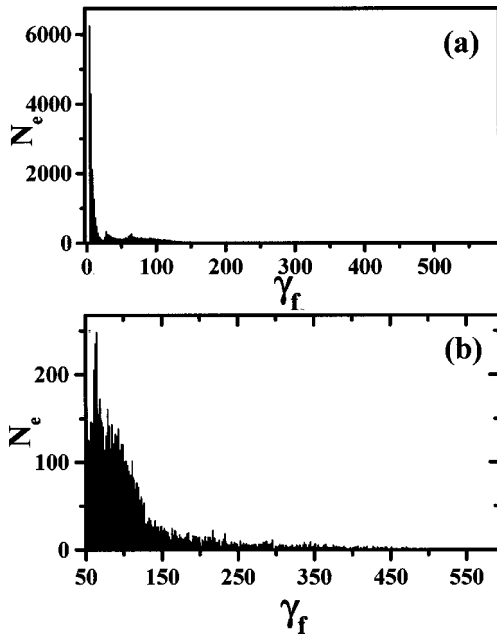


FIG. 11. (a) Electron energy spectra of the output electron bunch in Fig. 6(b). (b) The enlarged figure for the high-energy electron part in (a).

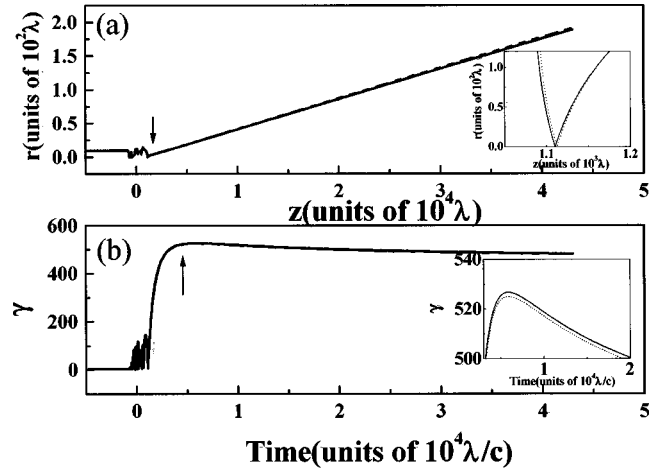


FIG. 12. The electron trajectory in the r - z plane (a) and the corresponding history of the electron energy (b) for a typical case of the electron trapping and acceleration by the TEM (1,0)+(0,1) mode laser are presented without (solid line) and with (dashed line) the radiation damping effect. The insets in (a) and (b) are the enlargements of the parts shown by arrows.

center of this high-energy cloud is located around $\gamma_f \sim 65$. The high-energy part represents the electrons trapped by the laser pulse and mostly belongs to the trapped electrons shown in Fig. 8.

In the above simulations, the influence of the electron radiation loss was ignored. In the relativistic limit the electron radiation damping effect can be evaluated by [31]

$$f = -\frac{2e^4}{3m_e^2 c^5} \gamma^2 \mathbf{v} [(\mathbf{E} + \boldsymbol{\beta} \times \mathbf{B})^2 - (\mathbf{E} \cdot \boldsymbol{\beta})^2]. \quad (21)$$

For the comparison we present one typical result employed in our present studies without (solid line) and with (dashed line) the radiation damping effect of Eq. (21) in Fig. 12. The laser parameters employed are $a_0 = 10$, $w_0 = 15\lambda$, and $L_z = 10\lambda$. The electron is injected with initial velocity $\beta_i = \beta_{zi} = 0.95$ from the initial position of $x_i = 4.15\lambda$, $y_i = 8.62\lambda$, and $z_i = -4775\lambda$. The difference of the final energy is $\Delta\gamma_f \sim 1.59$, and the radiation damping effect can be ignored in the cases treated in this paper, as is expected at this laser intensity.

C. The scaling law of the electron energy

It is also important to know the scaling law of the electron final energy. Normally the maximum electron net energy gained from the laser is proportional to $\gamma_0 a_0^2$ for the ponderomotive acceleration. For the longitudinal acceleration, following the analyses of Ref. [32], the energy exchange is estimated as $\Delta\epsilon \sim E_z Z_R \sim (2/kw_0) E_0 Z_R \sim a_0 w_0$. In Fig. 13(a) we present the maximum final electron energy $\gamma_{f \max}$ as a function of the laser intensity a_0 for $w_0 = 15\lambda$ and $L_z = 10\lambda$. One may see that for the lower intensity region, $a_0 < 10$, the relation $\gamma_{f \max} \propto a_0^2$ (shown by dashed line) holds well. However, for a higher intensity the scaling law seems to be different from a_0^2 but in the rule of a_0^n , where $1 < n < 2$.

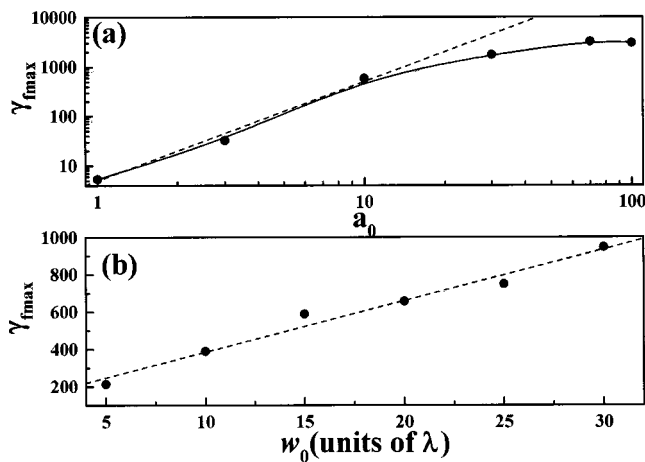


FIG. 13. (a) The scaling law between the maximum final electron energy $\gamma_{f \max}$ and the laser intensity a_0 . The parameters employed are $L_z=10\lambda$ and $w_0=15\lambda$. The electron initial velocity is $\beta_{xi}=\beta_{yi}=0.0$, $\beta_{zi}=0.95$ and the electron number is 16 000. The dashed line represents the relation of $\gamma_{f \max} \propto a_0^2$. (b) The scaling law between $\gamma_{f \max}$ and the laser spot size w_0 . The electron parameters are the same as in (a) and the laser parameters are $a_0=10$ and $L_z=10\lambda$.

Following the above analyses, the trajectories of the electrons trapping and acceleration in the TEM (1,0)+(0,1) mode laser are different from those in the usual ponderomotive acceleration. By the trapping effect, the electron can stay inside the strong field for a longer time. Consequently, the acceleration scaling law is not so simple. Because the trapping effect becomes more notable as the laser intensity increases, the scaling law of the maximum electron final energy may tend to stand apart from $\gamma_{f \max} \propto a_0^2$ at the higher laser intensity ($a_0 > 10$). Through our simulation studies we found that the electron can gain the maximum energy of about 1.55 GeV for $a_0=100$ with the following parameters:

$w_0=15\lambda$ and $L_z=10\lambda$ and the electron initial energy $\gamma_i=3.20$.

Another important parameter is the beamwidth, that is, the laser spot size at the laser focus point, i.e., w_0 . For the higher laser intensity, the maximum energy electron gain is proportional to w_0 : in Fig. 13(b) an example result is presented for the laser intensity of $a_0=10$ and $L_z=10\lambda$. In our simulations we also found that for a lower laser intensity, for example, $a_0=3$, the maximum energy electron gained does not depend on w_0 .

V. SUMMARY

In this paper, we investigated the ponderomotive acceleration in an intense short-pulse laser of TEM(1,0)+TEM(0,1) mode. In this scheme, the electrons are trapped effectively in the radial trap provided by this laser and stay in the strong-field region for a long time. During the trapping, the electron can be fully accelerated by the longitudinal ponderomotive force. For the electrons injected with the relativistic initial velocity and for the intense laser, the trapped electron can stay at the head of the laser pulse for a long time. As a result of this trapping effect, the electron bunch is confined in transverse by the laser to avoid the electron radial scattering, and at the same time compressed in longitudinal to the scale of the laser pulse duration. The high-energy and short-pulse electron bunch is successfully generated through this scheme, which may provide a viable electron bunch generator in the future.

ACKNOWLEDGMENTS

This work was partly supported by JSPS (Japan Society for the Promotion of Science). We would like to present our thanks to Professor K. Mima, Professor K. Tachibana, Professor S. Kurokawa, and Professor I. Pogorelsky for their fruitful discussions on this subject.

-
- [1] D. Strickland and G. Mourou, *Opt. Commun.* **56**, 219 (1985).
 [2] G. Mourou, C. P. J. Barty, and M. D. Perry, *Phys. Today* **51**(1), 22 (1998).
 [3] M. D. Perry *et al.*, *Opt. Lett.* **24**, 160 (1999).
 [4] R. Kienberger *et al.*, *Science* **297**, 1144 (2002).
 [5] D. Umstadter, S. Y. Chen, A. Maksimchuk, G. Mourou, and R. Wagner, *Science* **273**, 427 (1996).
 [6] J. R. Fontana and R. H. Pantel, *J. Appl. Phys.* **53**, 5435 (1982).
 [7] T. Tajima and J. M. Dawson, *Phys. Rev. Lett.* **43**, 267 (1979).
 [8] E. Esarey, P. Sprangle, M. Pillof, and J. Krall, *J. Opt. Soc. Am. B* **12**, 1695 (1995); E. Esarey, P. Sprangle, and J. Krall, *Phys. Rev. E* **52**, 5443 (1995).
 [9] B. Hafizi, A. Ting, E. Esarey, P. Sprangle, and J. Krall, *Phys. Rev. E* **55**, 5924 (1997); B. Hafizi, A. K. Ganguly, A. Ting, C. I. Moore, and P. Sprangle, *ibid.* **60**, 4779 (1999).
 [10] C. I. Moore *et al.*, *Phys. Rev. Lett.* **78**, 3314 (1997).
 [11] Y. I. Salamin and C. H. Keitel, *Appl. Phys. Lett.* **77**, 1082 (2000); Y. I. Salamin, F. H. M. Faisal, and C. H. Keitel, *Phys. Rev. A* **62**, 053809 (2002).
 [12] S. Kawata, T. Maruyama, H. Watanabe, and I. Takahashi, *Phys. Rev. Lett.* **66**, 2072 (1991).
 [13] P. X. Wang, Y. K. Ho, X. Q. Yuan, Q. Kong, N. Cao, A. M. Sessler, E. Esarey, and Y. Nishida, *Appl. Phys. Lett.* **78**, 2253 (2001); Q. Kong, Y. K. Ho, J. X. Wang, L. Feng, and Z. S. Yuan, *Phys. Rev. E* **61**, 1981 (2000).
 [14] F. V. Hartemann *et al.*, *Phys. Rev. E* **58**, 5001 (1998); **51**, 4833 (1995).
 [15] Y. Cheng and Z. Xu, *Appl. Phys. Lett.* **74**, 2116 (1999).
 [16] G. Malka and J. L. Miquel, *Phys. Rev. Lett.* **77**, 75 (1996); G. Malka, E. Lefebvre, and J. L. Miquel, *ibid.* **78**, 3314 (1997).
 [17] Q. Kong, S. Miyazaki, S. Kawata, K. Miyauchi, K. Nakajima, S. Masuda, N. Miyanaga, and Y. K. Ho, *Phys. Plasmas* **10**, 4605 (2003).
 [18] A. Boivin, E. Wolf, *Phys. Rev.* **138**, B156 (1965); J. K. McIver, Jr. and M. J. Lubin, *J. Appl. Phys.* **45**, 1682 (1974).
 [19] J. L. Chaloupka and D. D. Meyerhofer, *Phys. Rev. Lett.* **83**,

- 4538 (1999).
- [20] A. V. Gaponov and M. A. Miller, *Sov. Phys. JETP* **7**, 168 (1958).
- [21] C. I. Moore, *J. Mod. Opt.* **39**, 2171 (1992).
- [22] G. V. Stupakov and M. S. Zolotarev, *Phys. Rev. Lett.* **86**, 5274 (2001).
- [23] A. Yariv, *Optical Electronics*, 3rd ed. (Holt, Rinehart & Winston, New York, 1985).
- [24] Melvin Lax, William H. Louisell, and William B. McKnight, *Phys. Rev. A* **11**, 1365 (1975).
- [25] L. W. Davis, *Phys. Rev. A* **19**, 1177 (1979); J. P. Barton and D. R. Alexander, *J. Appl. Phys.* **66**, 2800 (1989).
- [26] N. Cao, Y. K. Ho, Q. Kong, P. X. Wang, X. Q. Yuan, Y. Nishida, N. Yugami, and H. Ito, *Opt. Commun.* **204**, 7 (2002).
- [27] Y. I. Salamin and F. H. M. Faisal, *Phys. Rev. A* **54**, 4383 (1998); *J. Phys. A* **31**, 1319 (1998).
- [28] K. McDonald and K. Shmakov, *Phys. Rev. ST Accel. Beams* **2**, 121301 (1999).
- [29] T. W. B. Kibble, *Phys. Rev. Lett.* **23**, 1054 (1966); T. Tajima, *Laser Part. Beams* **3**, 351 (1985).
- [30] M. Reiser, *Theory and Design of Charged Particle Beams* (Wiley-Interscience, New York, 1994).
- [31] L. D. Landau and E. M. Lifshits, *The Classical Theory of Fields* (Pergamon Press, Oxford, 1980).
- [32] M. O. Scully and M. S. Zubairy, *Phys. Rev. A* **44**, 2656 (1991).